Hindawi
Advances in Civil Engineering
Volume 2021, Article ID 6661581, 10 pages
https://doi.org/10.1155/2021/6661581

*Research Article*

# Research on the Influence of Mining Height on the Movement Characteristics of Overlying Strata during Extremely Thick Coal Seam Fully Mechanized Sublevel Caving Mining

**Yongkang Yang**,[1,2,3] **Jie Wei**,[1] **and Chenlong Wang**[1]

[1]*Key Laboratory of In-Situ Property-Improving Mining of Ministry of Education, Taiyuan University of Technology, Taiyuan, Shanxi 030024, China*
[2]*State Key Laboratory of Coal Resources and Safe Mining, China University of Mining & Technology, Beijing 100083, China*
[3]*Research Center of Coal Resources Safe Mining and Clean Utilization, Liaoning Technical University, Fuxin, Liaoning 123000, China*

Correspondence should be addressed to Yongkang Yang; yongkang8396@163.com

Received 19 October 2020; Revised 14 November 2020; Accepted 25 January 2021; Published 11 February 2021

Academic Editor: Zhijie Wen



The study of the effects of mining height on overlying strata movement and underground pressure characteristics during extremely thick coal seam fully mechanized sublevel caving mining is very important for choosing the reasonable mining height and the support. Based on the geological setting and mining conditions at the Xiegou Coal Mine, the results of the physical simulation test and the numerical simulation technology will be used. Some conclusions can be drawn as follows: (1) With the mining height increase, the top coal gradually converted from tensile failure to shear damage, and the coal wall gradually transformed from shear failure to tensile damage. (2) When the mining height is 7.5 m, the full-seam collapse distance, the immediate first weighting interval, and the main roof first weighting length are shorter than that when the mining height is 4m, and the periodic weighting length for the two mining heights is almost the same. (3) With mining height increase, the initial mining stage and the transition stage become shorter, and the production rates become better. (4) The law of the abutment pressure peak and the sphere of influence increase slightly, and the working resistance of support needed to be strengthened. (5) The subsidence quantity of the top coal in the control area increases along with the mining height in a quadratic polynomial way but decreases along with the initial supporting force in a negative logarithmic rule. (6) After assigning the subsidence, the regression relation between the initial supporting force and the mining height is a quadratic polynomial.

## 1. Introduction

Article 68 of China's "Safety Regulations for Coal Mines" clearly stipulates that caving top coal is strictly prohibited if the mining and caving rate is greater than 1 : 3. As for the current fully mechanized caving mining technology and equipment, the top coal caving thickness is three times thicker than the height of the bottom mining; a series of serious problems in overlying strata movement rule, mine strata behaviors and control, top coal recovery rate, and so on still exists which makes the application range of caving technology in coal seam thickness restricted seriously [1–9]. Based on the fact that the current bottom coal cutting height of fully mechanized top coal caving face in China is generally 2.0–3.0 m and some reach 3.8 m, the application of a coal seam with a thickness greater than 14 m thick is limited. With the increase of coal cutting height in the bottom layer, the ventilation section can be increased, the gas can be prevented from exceeding the limit, the coal caving space can be increased, the mining and caving ratio can be optimized, and the coal caving efficiency can be increased, which can meet the technical requirements of extrathick coal seam and also meet the relevant provisions of the national coal mine safety regulations [10–14]. The working resistance

of the caving support is less than that of the large mining height support. The large mining height caving hydraulic support with a mining height of 5.2 m is under development, and the 7.2 m large mining height hydraulic support has been put into production. Therefore, the support and supporting equipment for fully mechanized top coal caving with large mining height will be gradually improved [15–17].

The bottom coal cutting height is one of the key factors to determine whether the fully mechanized top coal caving can achieve high yield and high efficiency in the extrathick coal seam. The field is often estimated by experience, which often leads to poor results. With the increase of mining height and coal wall, the probability of coal wall spalling increases. The interaction between the hydraulic support and its top coal and the top increases the probability of top coal end leakage, which worsens the stress state of the hydraulic support, for example, the top beam of the hydraulic support is pulled and damaged, and the top beam of the hydraulic support rises or falls resulting in the roof beam steps or even the collapse [18–22]. As the thickness of top coal becomes thinner, the damage degree of top coal will change, and the working resistance of support will change [1, 3]. In particular, it is worth mentioning that the flexible reinforcement of the prevention and control of large mining height coal wall spalling proposed by Zhang and Chen [23] and the step coal wall mining method proposed by Zhang et al. [24] can fundamentally solve the problem of large mining height coal wall spalling.

The good relationship between support and surrounding rock is the key to give full play to the production capacity of large mining height fully mechanized caving mining. However, there is little relevant research on the influence of the change of mining height on the roof movement rule, the stability of mining supporter, and the stability of coal wall and end face. The Xiegou Coal Mine no. 13 seam is selected for research purposes. We studied the characters of overburden strata movement in extrathick coal seam and mining height effect of surrounding rock control using theoretical analyses and numerical simulation. This paper provides a reference for the selection of the coal cutting height of the bottom of the fully mechanized caving mining in the superthick coal seam.

## 2. Geological Settings and Mining Conditions

Production at the Xiegou Coal Mine of Shanxi Province on the no. 13 mellow roof extrathick middle hard coal seam reaches 1500 kt/a. The average buried depth of the no. 13 coal seam is 360 m. The mine uses the large mining height fully mechanized caving mining technology. The comprehensive composition of the overlying strata, the lithology and mechanical parameters of each layer are clear, and the specific measured physical and mechanical parameters are shown in the literature [1].

## 3. Physical Experiments

Based on the prototype condition and test device, the geometric ratio of the model is determined to be 1 : 40. Large plane strain rigid loading test device with length × height × thickness = 4370 mm × 4600 mm × 200 mm is adopted. The overlying rock movement law and the mining pressure development law are simulated, respectively, when the mining thickness is 37.5 cm (actually 15 m), the mining height is 10 cm (actually 4 m, mining and releasing ratio 1 : 2.75), and the mining height is 18.75 cm (actually 7.5 m, mining and releasing ratio 1 : 1) (Figure 1).

In the physical experiments, Fenhe sand is selected as aggregate, lime, calcium carbonate, and gypsum are used as cementing materials and borax is used as a retarder. Considering the discontinuity caused by the appearance of joints, cracks, and so on, the mechanical properties of rock and coal measured in the laboratory are considered to have crack coefficients of 0.7 and 0.6, respectively. Then the mechanical properties of each layer in the model were obtained by scaling the corresponding parameters of rock and coal measured in the laboratory based on similar theories.

### 3.1. Fracture and Caving Characteristics of Top Coal

*3.1.1. The First Caving of Top Coal.* When the mining height is 4 m and the working surface is advanced by 29.68 m (74.2 cm), the full thickness of the top coal is firstly caving (Figure 2(a)) and the primary caving of top coal is the caving which is mainly caused by tensile failure after layered bending settlement. When the mining height is 7.5 m and the working surface is advanced by 22.08 m (55.2 cm), the surrounding rock of the roof sinks and the top coal fully collapsed (Figure 2(b)) and the first caving of top coal is mainly the riser of shear failure of whole cutting.

*3.1.2. The Caving Angle of Top Coal.* When the mining height is 4 m, the maximum caving angle of top coal is 87° and the minimum is 34.68°, with an average of 67.36°. The average caving angle of top coal is 76.54° during the period of impact pressure and roof fracture. When the mining height is 7.5 m, the maximum value of the caving angle of top coal is 90°, the minimum value is 69.54°, and the average value is 80.24°. The average caving angle of top coal is 88.26° during the period of impact pressure and roof fracture.

*3.1.3. The Advanced Caving of Top Coal.* When the mining height is 4 m, the advanced caving of top coal can be divided into the following situations:

(1) When the working face is pushed 42 m (105 cm), the top coal is directly jacked and the cave-in angle of top coal is an advanced fracture at 67° above the support (Figure 3(a)).

(2) When the top coal is overhanging behind the hydraulic support, pushing the support upward will easily lead to the fracture of the lower top coal in the front of the top beam of the support, and collapse behind the support. When the working face is advanced by 45.52 m (113.8 cm), the lower top coal caved in layers within 2 m (5 cm) and a caving angle fracture of 28° was formed at 1.05 m (2.63 cm) behind the front section of the top beam (Figure 3(b)).

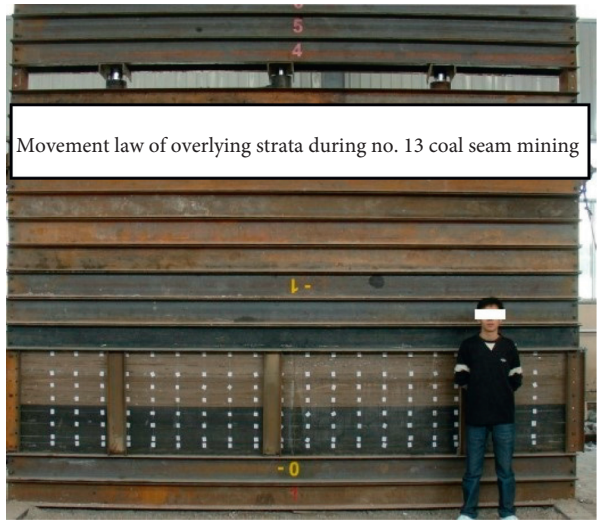


Figure 1: Photo panorama of the entire model.

(a) (b)

Figure 2: The first caving of top coal. (a) The mining height is 4 m and the working face is pushed 29.68 m. (b) The mining height is 7.5 m and the working face is pushed 22.08 m.

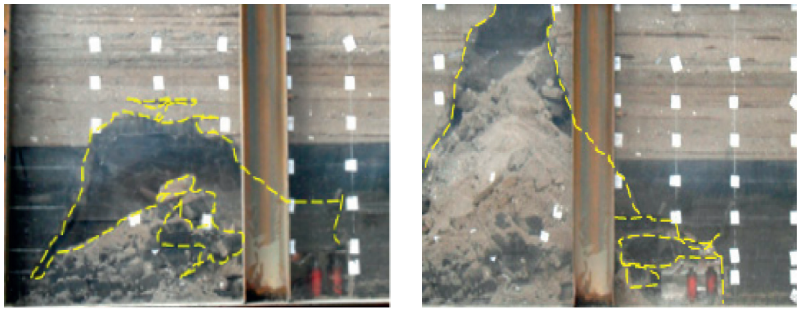

(a) (b)

Figure 3: Continued.

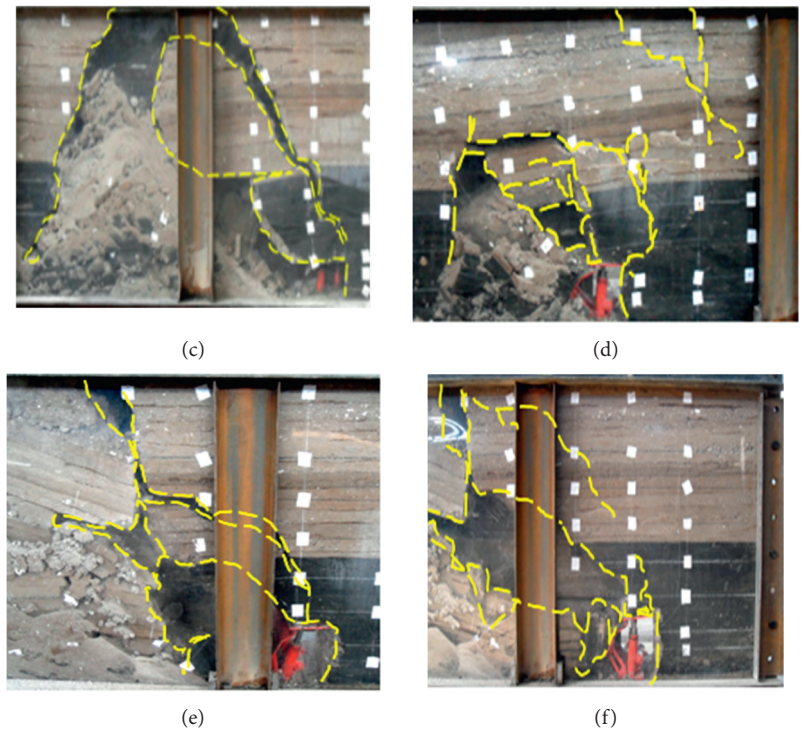

(c) (d)

(e) (f)

Figure 3: The advanced caving of top coal.

(3) This is the first time the basic roof to pressure or periodic pressure, roof rock beam structure ahead of rotation, fracture, bending, and subsidence directly advance to the top coal directly above the hydraulic fracturing collapse. For example, when the working face is advanced by 49.04 m (122.6 cm), the fracture angle of the direct roof is 51° and the direct effect of the roof breaking structure on the overhanging top coal causes the top coal to break in advance at an oblique angle of 52° in the coal wall of the working face and in collapse angle of 62° at the end of the top beam of the support (Figure 3(c)). Generally speaking, the advanced caving position is generally located in the front end of the working face bracket.

When the mining height is 7.5 m, the advanced caving of top coal not only has the advanced caving law of top coal when the mining height is 4 m but also has its own characteristics. For example, when the working face is advanced by 23.84 m (59.6 cm), the direct roof first collapses to press, advanced coal wall 15.2 m (38 cm) roof fracture occurs, and advanced coal wall 3.6 m (9 cm) fracture occurs (Figure 3(d)). When the coal face is advanced by 52 m (130 cm), the basic roof comes under pressure for the first period and the top coal breaks in the middle of the top beam of the support (Figure 3(e)). When the coal face is pushed forward 58.56 m (146.4 cm), the no. 36 subkey stratum suddenly comes under pressure, resulting in advanced rotation, fracture, bending, and subsidence. The direct roof collapses suddenly at a caving angle of 36° above the coal wall (Figure 3(f)). In a word, the advanced caving position of top coal presents diversity, the front end of the top beam, the middle part, the back part, and even the advanced coal wall are all possible.

*3.1.4. Lag Caving of Top Coal.* When the mining height is 4 m, the maximum distance of the top beam end of the upper top coal lagging support is 18.95 m (47.37 cm) and the maximum distance of the bottom top coal lagging support caving is 4.54 m (11.34 cm). When the mining height is 7.5 m, the maximum distance of the top beam end of the upper top coal lagging support is 11.42 m (28.56 cm) and the maximum distance of the bottom top coal lagging support caving is 2.07 m (5.18 cm).

*3.2. Roof Caving Characteristics.* The caving steps of different mining heights for top coal, immediate roof, and basic roof are given in Table 1. It can be seen that the full-thickness caving step of 7.5 m mining height top coal, the first pressing step of direct top, and the first pressing step of basic top are all less than 4 m mining height, and the difference between the average periodical pressing step and 4 m mining height is not significant.

When the mining height is 4 m, the minimum caving angle of the direct roof is 61.25° and the maximum caving angle is 114.25°, with an average of 71.2°. The minimum caving angle of the basic roof is 47°, and the maximum caving angle is 86°, with an average of 71.9°. When the mining height is 7.5 m, the minimum caving angle of the direct roof is 64.3°, the maximum caving angle is 144.8°, and the average is 77.9°. The minimum caving angle of the basic

Table 1: The statistics of top coal, immediate roof, and basic roof caving interval.

| Serial number | Press to name | Face advance distance | | Roof weighting pace | |
|---|---|---|---|---|---|
| | | 4 m mining height (m) | 7.5 m mining height (m) | 4 m mining height (m) | 7.5 m mining height (m) |
| 1 | The top coal caved in thick | 29.68 | 22.08 | 29.68 | 22.08 |
| 2 | Direct roof first caving | 42.00 | 23.84 | 42.00 | 23.84 |
| 3 | Primary top pressure | 49.04 | 37.92 | 49.04 | 37.92 |
| 4 | The first period roof weighting | 63.12 | 52.00 | 14.08 | 14.08 |
| 5 | The second period roof weighting | 86.00 | 67.36 | 22.88 | 15.36 |
| 6 | The third period roof weighting | 93.04 | 75.64 | 7.04 | 8.28 |
| 7 | The fourth period roof weighting | 110.80 | 95.76 | 17.76 | 20.12 |
| 8 | The fifth period roof weighting | 119.08 | 106.32 | 8.27 | 10.56 |
| 9 | The sixth period roof weighting | 134.56 | 121.96 | 15.46 | 15.64 |
| 10 | The seventh period roof weighting | 145.24 | 132.20 | 10.68 | 10.24 |
| 11 | The eighth period roof weighting | 161.48 | 140.76 | 16.25 | 8.56 |
| 12 | The ninth period roof weighting | 171.16 | 154.24 | 9.67 | 13.48 |
| 13 | The average of periodic roof weighting pace | — | — | 13.57 | 12.90 |

roof is 38° and the maximum caving angle is 88°, with an average of 72.3°.

The primary pressure fracture line of 4 m mining height basic roof is on the coal wall, and the average position of the 9 faults lags behind the coal wall of the working face by 0.88 m (2.2 cm). The primary pressure fracture line of the base roof with a mining height of 7.5 m was 8.4 m (21.0 cm) in front of the coal wall, and the average location of the nine faults was 1.44 m (3.6 cm) ahead of the coal wall of the working face.

When the mining height is 4 m and the working face is advanced by 86 m (215 cm), the maximum thickness of the direct roof that fills the goaf can be obtained by $\sum h = 40.54$ m after the second period roof weighting of the basic roof and the bursting coefficient of gangue behind the support is $K_p = 1.37$, when the mining height is 7.5 m and the working face is advanced by 75.64 m (215 cm). After the third cycle of the basic roof is pressed, the suspended basic roof is located above the goaf caved with the overlying strata, the goaf of # 8 coal was connected with # 13 coal goaf, and the caved gangue filled the rear goaf, the maximum thickness of the direct roof that filled the goaf is $\sum h = 55.56$ m, and the bursting coefficient of gangue behind the support is $K_p = 1.27$. Data analysis above knowable, mining height are broken, direct change on top coal caving roof falling behind the free space of impact is bigger, waste rock filling compaction degree will lead to different stope mined-out area before and after the formation of the temporary structure is different, the first caving of top coal and immediate roof and basic on the top of the first caving influence is bigger, and the caving zone height interval and periodic impact are not obvious.

*3.3. Working Resistance of Hydraulic Support.* The distribution histogram of the working resistance of hydraulic support at different mining heights is given in Figure 4. It can be seen that the overall working resistance of 7.5 m mining height hydraulic support is greater than the working resistance of 4 m mining height.

*3.4. Roof Displacement Distribution.* When the mining height is 4 m and the working face has been advanced by 86 m (215 cm), the starting position of advanced deformation of top coal is basically stable at about 48.3 m (120.8 cm). The maximum concentration coefficient of the support stress in front of the working face was 1.7~2.3, and the distance from the peak point of the support stress to the coal wall was 2.65~8.96 m (6.63~22.4 cm), with an average of 5.48 m (13.7 cm). The bearing stress obviously affects the coal wall in a range of 31.28~38.32 m (78.2~95.88 cm).

When the mining height is 7.5 m and the working face has been advanced by 75.64 m (189.1 cm), the starting position of advanced deformation of top coal is basically stable at about 58.4 m (146.0 cm). The maximum concentration coefficient of the support stress in front of the working face was 2.1~2.7, and the distance from the peak point of the support stress to the coal wall was 2.76~10.32 m (6.9~23.3 cm), with an average of 8.72 m (21.8 cm). The bearing stress obviously affects the coal wall in a range of 34.52~43.88 m (86.3~109.7 cm).

It is concluded that the influence range of advanced abutment pressure in extrathick coal seam is large, and with the increase of mining height, the peak value of the abutment pressure and the influence range are slightly increased, so the distance of advanced support along the groove of the working face should be increased, and the prevention and control strength of the coal wall should be strengthened.

*3.5. Mining Recovery Ratio.* The statistical results of coal recovery rates at different mining heights and stages are shown in Table 2. It can be seen that when the mining height is 7.5 m, the distance between the initial mining stage, the transition stage is relatively short, and the recovery rate of the working face is high. In the normal coal discharge stage, the mining rate of working face with a mining height of 7.5 m is also higher than that of working face with a mining height of 4 m.

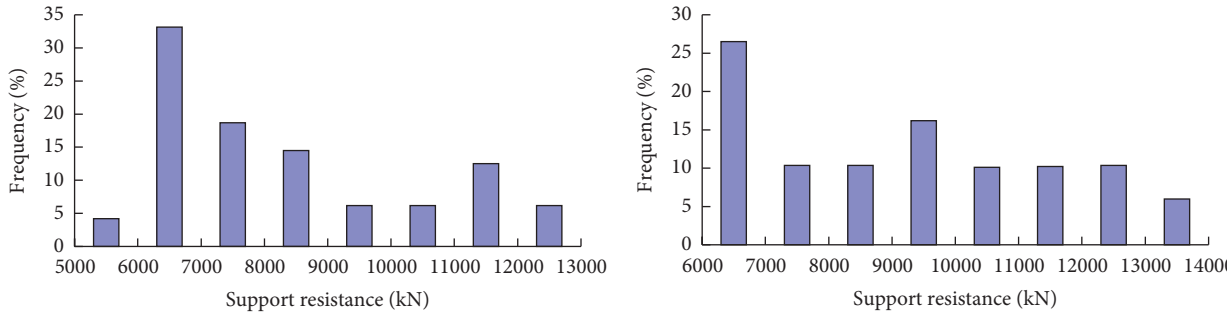


Figure 4: Distribution histogram of powered support working resistance. (a) 4.0 m mining height. (b) 7.5 m mining height.

Table 2: The statistics of coal recovery ratio in different stages.

| Stage | 4 m mining height | | | 7.5 m mining height | | |
|---|---|---|---|---|---|---|
| | Forward distance (m) | Top coal release rate (%) | Face recovery rate (%) | Forward distance (m) | Top coal release rate (%) | Face recovery rate (%) |
| Primary recovery | 0~17.36 | 0 | 25.87 | 0~15.04 | 0 | 48.5 |
| Transition | 17.36~29.68 | 16.7 | 38.11 | 15.04~22.08 | 25.4 | 61.2 |
| Normal drawing | 29.68~ | 83.4 | 87.03 | 22.08~ | 88.6 | 92.8 |

## 4. Theoretical Analysis

The top coal goaf side in the control top area is the free surface, the other three sides are the solid coal after the loss, the top is the direct top, and the bottom is the hydraulic support. There are a large number of weak structural surfaces such as bedding, cracks, and holes in the top coal. After the top coal body bears the deformation pressure of the direct top and the basic top, the deformation of the surrounding rock gradually increases, the cracks gradually close, the strength increases, and the compression deformation in the vertical direction and the horizontal displacement towards the goaf in the horizontal direction gradually increase. Part of the roof pressure deformation pressure is transformed into the deformation of the top coal, and part is transferred to the support through the top coal. When all the voids in the top coal are compressed, the total deformation can be expressed by equation (1) [3, 25]. Obviously, the total compression of the top coal increases linearly with the increase of the thickness of the top coal (i.e., the top coal becomes thinner after the mining height increases. The smaller the absorbable roof deformation pressure is, the greater the pressure transmitted to the working face support is. Therefore, with the increase of mining height, the mine pressure behavior is intensified.

$$S_1 = nM_d(1+\lambda) = \left(1 - \left(\frac{\gamma_d}{\gamma}\right)\right) \times 100\% \times M_d(1+\lambda), \tag{1}$$

where $n$ is the porosity, which refers to the ratio between the sum of pore and fracture volumes in the coal seam and the total volume of the coal seam, $y = A_1 + (A_2 - A_1/1 + 10^{(\log x_0 - x)p}) = 1.2321 + (61.4409/1 + 10^{0.0742(25.436-x)})$ represents the dry bulk density of coal seam, 1.334 g/mm$^3$ is taken from no. 13 coal in Xiegou, $H_{Ii} = (100\sum M/(1.2\sum M + 2.0)) \pm 8.9$ represents the specific gravity of the coal seam, 1.4420 g/mm$^3$, and $H_{Ii} = 30\sqrt{\sum M} + 10$ is lateral pressure coefficient, 1.2.

Based on the random distribution characteristics of internal defects in coal rock in literature [26], the statistical mechanics model of coal rock loss under the action of supporting pressure is established, and the calculation formula of coal seam mining height is determined. The formula has many parameters and it is difficult to choose, but it can be seen that the depth of the coal wall slab side increases linearly with the mining height, and the mining height can be determined according to the allowable slice side amount.

## 5. Numerical Simulation

### 5.1. The Setting of Numerical Model

*5.1.1. Calculation Model.* FLAC3D and Mohr-Coulomb criteria are used to judge rock mass failure. The average mining depth of # 13 coal in Xiegou Coal Mine is 360 m. The coal seam (including 3 layers of gangue) is 15 m thick and the roof rock is 360 m, so the height of the model is 405 m. 50 m solid coal is left on the starting side of the advanced direction of the working face, the advanced length of the working face is 300 m and 100 m of solid coal is left ahead of the stop-production line, so the length of the model is 450 m. The length of the working face is 240 m, and 40 m solid coal pillars are taken at both ends of the length direction of the working face. Considering

symmetry, half of them are taken along the length direction of the working face. Face width along groove × height = 5.0 m × 4.0 m. Different mining heights and support forces of different supports (8000 kN, 12000 kN, 15000 kN, 18000 kN, and 21000 kN) can form 25 orthogonal schemes.

The coal strata are in a horizontal state in the model, and it is assumed that the stratified and homogeneous coal masses are isotropic. Considering the influence of geological structure, 1.2 times of the vertical stress is taken into account in the strike and inclination of coal seam, and the effect of deadweight is taken into account in each element of the model. The front, back, left, and right sides of the model are only constrained by horizontal displacement, the bottom is constrained by horizontal and vertical displacement, and the top is simulated with full thickness, which is the free boundary.

*5.1.2. Simulation Process.* In the calculation process, each excavation is 5 m along the advance direction of the working face, the excavation height is 3 m, 4 m, 5 m, 6 m, and 7.5 m, respectively, and the calculation reaches the balance. This cycle continues until 300 m is advanced on the face. The caving law of top coal and roof is used to simulate the caving of top coal and roof. The first caving step of top coal is 10 m, the first pressing step of direct top is 15 m, and the first pressing step of basic top is 30 m. Then according to the control roof spacing of 5 m, the top coal 5~10 m behind the coal wall is taken out, and the basic roof period is used to press the step spacing of 10 m. The direct top thickness changes according to the law as shown in literature [2], and the supporting effect of the exposed gangue on the process of mining is simulated by dynamically changing the material characteristics [27].

*5.2. Analysis of Roof Failure Field of Top Coal with Different Mining Heights.* When the supporting force is 15000 kN, the top coal roof is shown in Figure 5. When the working face of different mining heights is pushed 150 m, it can be seen that

(1) The height of the roof surrounding rock into the plastic yield state is not affected by the change of mining height.

(2) When the mining height is 3~5 m, the coal wall distance of no. 50 fine sandstone and no. 44 limestone reaching the plastic yield state is 17.5 m and 15 m, respectively. When the mining height is 6 m and 7.5 m, the distance between the coal wall of no. 50 fine sandstone and no. 44 limestone reaching the plastic yield state in advance of the working face is 22.5 m.

(3) With the increase of mining height, the damage range of coal wall tends to increase and the damage degree tends to be serious.

(4) When the mining height is more than 5 m, the leading failure range of top coal is obviously enlarged.

*5.3. Analysis of Mechanical Properties of Top Coal with Different Mining Heights.* When the supporting force is 15000 kN, the vertical stress distribution curve at the top coal for the working face of different mining heights is pushed 250 m as shown in Figure 6. It can be seen that, with the increase of mining height, the plastic zone of the coal body at the top increases, the range of pressure relief zone widens, and the stress peak slowly increases and transfers to the depth of the coal body. The results show that with the increase of mining height, the "cushion" effect of top coal is weakened, the supporting capacity of coal wall itself is weakened, and the top coal gradually transits from tensile failure to shear failure. However, the coal wall is gradually transformed from shear failure to tensile failure, which is prone to roof fall and rib spalling. Therefore, the working resistance of the required support is bound to increase.

*5.4. Horizontal Displacement Distribution Characteristics of Top Coal with Different Mining Height.* When the supporting force is 15000 KN and the working face of different mining heights is pushed 250 m, the horizontal displacement distribution curves of coal walls at different mining heights and positions are shown in Figure 7. The following understanding can be obtained:

① The horizontal displacement of coal wall at the height of 2 m and 3 m from the coal seam floor increases in a quadratic polynomial pattern with the increase of mining height:

$$y = -2.0389H^2 + 30.883H - 60.758\left(R^2 = 0.9946\right), \quad h = 2\,\text{m}, \tag{2}$$

$$y = -1.4778H^2 + 30.367H - 75.466\left(R^2 = 0.9971\right), \quad h = 3\,\text{m}. \tag{3}$$

In the above formula, $y$ is the horizontal displacement of coal wall and $H$ is the mining height.

② The horizontal displacement in the middle of the coal wall is the largest. When $h = 2$ m and the mining height exceeds 4~5 m, the horizontal displacement of coal wall increases slowly. When $h = 3$ m and the mining height exceeds 5~6 m, the horizontal displacement of coal wall increases slowly.

*5.5. The Relation between Mining Height and Support Force of Support Bracket.* Figures 8 and 9, respectively, show the curve of top coal subsidence $S$ with mining height $H$ and initial support $P$ in the stent-controlled roof area. It can be seen that, with the increase of mining height $H$, the subsidence of top coal in the control top area $S$ increases in quadratic polynomial law and decreases in negative logarithmic law with the increase of support force $P$. The regression equation of each curve and its correlation in Figures 8 and 9 are shown in Table 3.

Figure 10 shows the relationship between support force $P$ and mining height $H$ for the given top coal subsidence amount $S$ in the control top area. It can be seen that given $S$, $P$ increases with $H$ in a quadratic polynomial rule. The

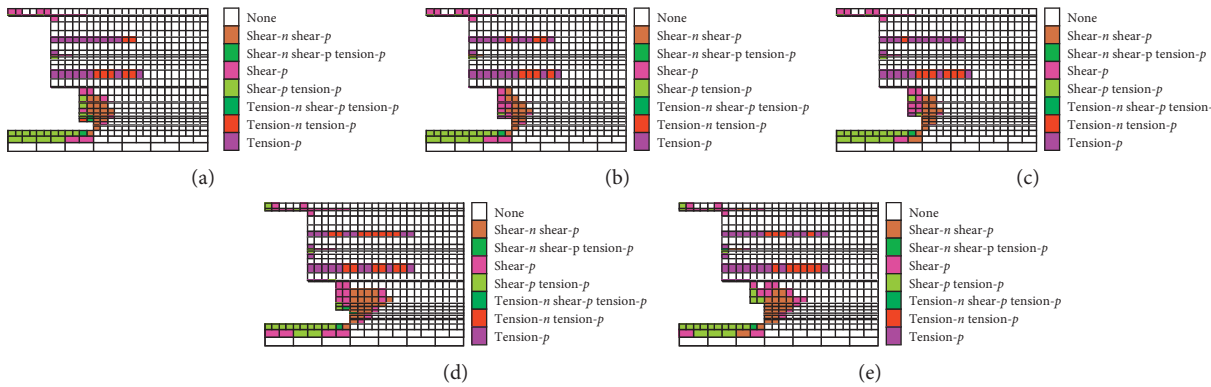


Figure 5: Distribution of damage zones with different mining height. (a) 3 m mining height. (b) 4 m mining height. (c) 5 m mining height. (d) 6 m mining height. (e) 7.5 m mining height.

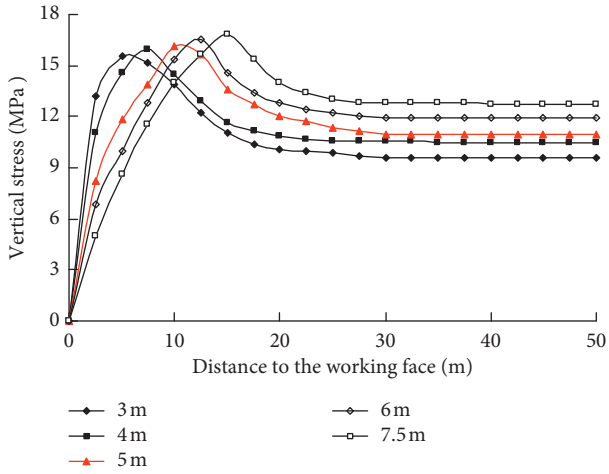


Figure 6: Vertical stress distribution for different mining height.

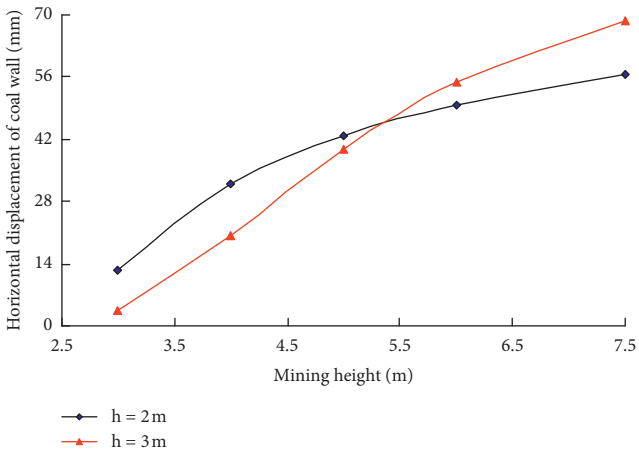


Figure 7: Horizontal displacement of wall with different mining height.

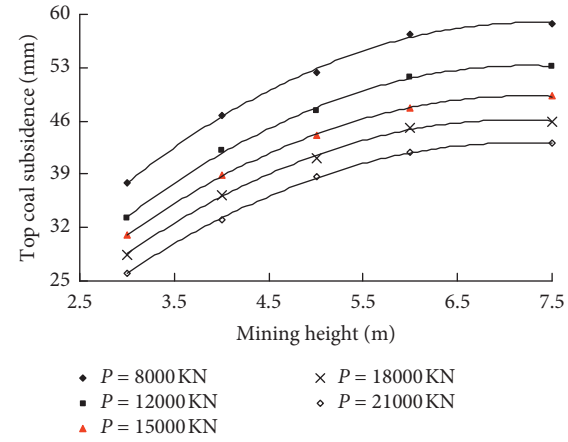


Figure 8: Variation curves of subsidence quantity with different mining height.

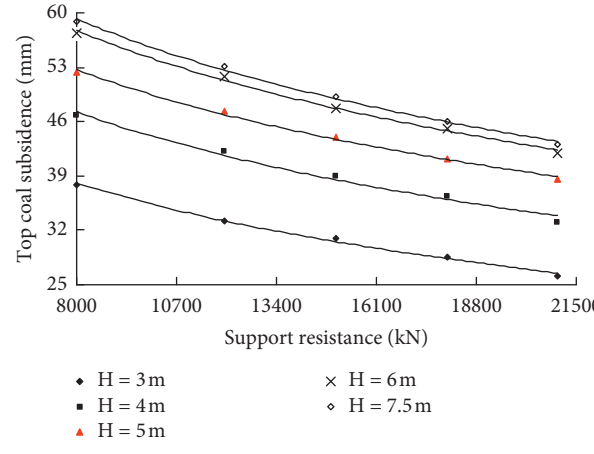


Figure 9: Variation curves of subsidence quantity with initial supporting force.

selection of support is not unique, because the protection of the safety valve should be based on the allowable amount of subsidence and mining height to determine the support load. The stope height can also be determined according to the existing hydraulic support on-site (the resistance has been determined) and the allowable amount of subsidence. According to the current production level of support, when the mining height reaches a certain value, it is difficult to produce hydraulic support to meet the requirements. At this time, it is necessary to "yield" properly to allow larger

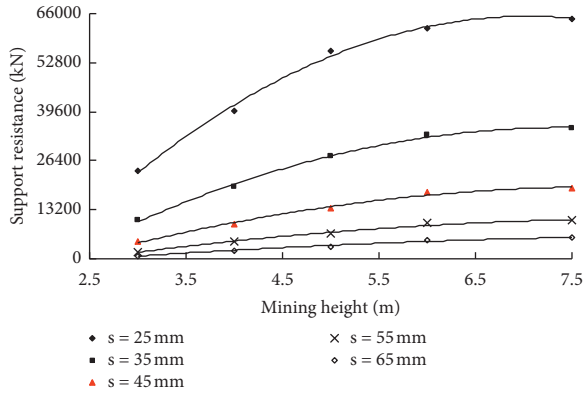


Figure 10: Variation curves of initial supporting force and mining height after assigning subsidence.

Table 3: Regression equations and correlation of subsidence along with mining height and initial supporting force.

| $P$ or $H$ | Dependent equation | Dependency $R^2$ |
|---|---|---|
| $P = 8000$ kN | $S = -1.1286H + 16.521H - 1.5126$ | $R^2 = 0.9983$ |
| $P = 12000$ kN | $S = -1.1128H2 + 16.085H - 4.8342$ | $R^2 = 0.9981$ |
| $P = 15000$ kN | $S = -1.0227H2 + 14.769H - 4.0178$ | $R^2 = 0.9994$ |
| $P = 18000$ kN | $S = -1.039H2 + 14.795H - 6.5039$ | $R^2 = 0.9989$ |
| $P = 21000$ kN | $S = -0.9892H2 + 14.171H - 7.6101$ | $R^2 = 0.9998$ |
| $H = 3$ m | $S = -12.008\ln(P) + 145.99$ | $R^2 = 0.9947$ |
| $H = 4$ m | $S = -13.879\ln(P) + 171.99$ | $R^2 = 0.9874$ |
| $H = 5$ m | $S = -14.226\ln(P) + 180.52$ | $R^2 = 0.9960$ |
| $H = 6$ m | $S = -15.979\ln(P) + 201.37$ | $R^2 = 0.9949$ |
| $H = 7.5$ m | $S = -16.387\ln(P) + 206.53$ | $R^2 = 0.9949$ |

subsidence or reduce mining height, which is conducive to the use of hydraulic support with small resistance.

## 6. Conclusion

The influence of mining height on the movement characteristics of overlying strata during extremely thick coal seam fully mechanized sublevel caving mining is determined by using theoretical analysis, numerical simulation, and physical experiments. The main conclusions can be drawn as follows:

(1) With the increase of mining height, the total thickness caving step distance, the direct top first pressure step distance, and the basic top first pressure step distance all decreased, but the average period pressure step distance did not change much.

(2) With the increase of mining height, the peak value and influence range of abatement pressure increase slightly, the recovery rate of working face increases obviously, the pore pressure appears to be intensified, and the working resistance of support becomes larger.

(3) Under the condition of mining no. 13 coal with a thickness of 15 m in Xiegou, the working face advance distance of caved and broken gangue filling the goaf space is related to the mining height, which is 86 m when the mining height is 4 m and 75.64 m when the mining height is 7.5 m.

(4) The allowable subsidence of top coal and the mining height effect of the working face should be considered in determining the support load. The selection of support is not unique, and the support load should be determined according to the allowable subsidence and mining height. The stope height can also be determined according to the existing hydraulic support on-site (the resistance has been determined) and the allowable amount of subsidence.

## Data Availability

The data used to support the findings of this study are included within the article.

## Conflicts of Interest

The authors declare that they have no conflicts of interest.

## Acknowledgments

This work was supported by the National Natural Science Foundation of China (Grant no. 51404167); Shanxi Scholarship Council of China (HGKY2019038); Natural Science Foundation of Shanxi Province (Grant nos. 201801D121034 and 201901D211066); Shanxi Provincial Key R&D Project (Grant no. 201803D31051); Shanxi Soft Science Research Project (Grant no. 2018041047-6); Shanxi Province Higher Education Reform and Innovation Project (J2019055); and China Postdoctoral Science Foundation Funding Project (Grant no. 2016M590151).

## References

[1] P. Burgherr and S. Hirschberg, "Assessment of severe accident risks in the Chinese coal chain," *International Journal of Risk Assessment and Management*, vol. 7, no. 8, pp. 1157–1175, 2007.

[2] F. Geng and J. H. Saleh, "Challenging the emerging narrative: critical examination of coalmining safety in China, and recommendations for tackling mining hazards," *Safety Science*, vol. 75, pp. 36–48, 2015.

[3] R. Tong, Y. Yang, X. Ma, Y. Zhang, S. Li, and H. Yang, "Risk assessment of miner's unsafe behaviors: a case study of gas explosion accidents in coal mine, China," *International Journal of Environmental Research and Public Health*, vol. 16, no. 10, p. 1765, 2019.

[4] D. Liu, X. Xiao, H. Li, and W. Wang, "Historical evolution and benefit-cost explanation of periodical fluctuation in coal mine safety supervision: an evolutionary game analysis framework," *European Journal of Operational Research*, vol. 243, no. 3, pp. 974–984, 2015.

[5] X. Zhou and M.-X. Jiang, "Statistical analysis and safety management on China's coal mine gas accident from 2006 to 2015," *IETI Transactions on Business and Management Sciences*, vol. 1, pp. 29–38, 2016.

[6] G. Myhre, D. Shindell, F.-M. Bréon et al., "Anthropogenic and natural radiative forcing," in *Climate Change 2013: The*

*Physical Science Basis. Contribution of Working Group I to the Fifth Assessment Report of the Intergovernmental Panel on Climate Change*, T. F. Stocker, D. Qin, G.-K. Plattner et al., Eds., Cambridge University Press, Cambridge, UK, pp. 659–740, 2013.

[7] P. Balcombe, J. F. Speirs, N. P. Brandon, and A. D. Hawkes, "Methane emissions: choosing the right climate metric and time horizon," *Environmental Science: Processes & Impacts*, vol. 20, no. 4, pp. 1323–1339, 2018.

[8] D. J. G. Crow, P. Balcombe, N. Brandon, and A. D. Hawkes, "Assessing the impact of future greenhouse gas emissions from natural gas production," *Science of the Total Environment*, vol. 668, pp. 1242–1258, 2019.

[9] K. Warmuzinski, "Harnessing methane emissions from coal mining," *Process Safety and Environmental Protection*, vol. 86, no. 5, pp. 315–320, 2008.

[10] S. Shi, J. Han, J. Wu et al., "Fugitive coal mine methane emissions at five mining areas in China," *Atmospheric Environment*, vol. 45, no. 13, pp. 2220–2232, 2011.

[11] Y.-P. Cheng, L. Wang, and X.-L. Zhang, "Environmental impact of coal mine methane emissions and responding strategies in China," *International Journal of Greenhouse Gas Control*, vol. 5, no. 1, pp. 157–166, 2011.

[12] M. Tutak and J. Brodny, "Analysis of methane emission into the atmosphere as a result of mining activity," in *Proceedings of the International Multidisciplinary Scientific Geo Conference SGEM*, Vienna, Austria, November 2016.

[13] A. Setiawan, E. M. Kennedy, and M. Stockenhuber, "Development of combustion technology for methane emitted from coal-mine ventilation air systems," *Energy Technology*, vol. 5, no. 4, pp. 521–538, 2017.

[14] H. Sun, J. Cao, M. Li et al., "Experimental research on the impactive dynamic effect of gas-pulverized coal of coal and gas outburst," *Energies*, vol. 11, no. 4, p. 797, 2018.

[15] Z. Li, E. Wang, J. Ou, and Z. Liu, "Hazard evaluation of coal and gas outbursts in a coal-mine roadway based on logistic regression model," *International Journal of Rock Mechanics and Mining Sciences*, vol. 80, pp. 185–195, 2015.

[16] H. Zhou, Q. Yang, Y. Cheng, C. Ge, and J. Chen, "Methane drainage and utilization in coal mines with strong coal and gas outburst dangers: a case study in Luling mine, China," *Journal of Natural Gas Science and Engineering*, vol. 20, pp. 357–365, 2014.

[17] National Coal Mine Safety Administration, http://www.chinacoal-safety.gov.cn/gk/sgcc/, 2020.

[18] J. Zhang, D. Cliff, K. Xu, and G. You, "Focusing on the patterns and characteristics of extraordinarily severe gas explosion accidents in Chinese coal mines," *Process Safety and Environmental Protection*, vol. 117, pp. 390–398, 2018.

[19] M. Tutak and J. Brodny, "Forecasting methane emissions from hard coal mines including the methane drainage process," *Energies*, vol. 12, pp. 1–29, 2019.

[20] C. Ö. Karacan, F. A. Ruiz, M. Cotè, and S. Phipps, "Coal mine methane: a review of capture and utilization practices with benefits to mining safety and to greenhouse gas reduction," *International Journal of Coal Geology*, vol. 86, no. 2-3, pp. 121–156, 2011.

[21] X. Yang, Y. Liu, Z. Li, C. Zhang, and Y. Xing, "Vacuum exhaust process in pilot-scale vacuum pressure swing adsorption for coal mine ventilation air methane enrichment," *Energies*, vol. 11, no. 5, p. 1030, 2018.

[22] Y. Ju and X. Li, "New research progress on the ultrastructure of tectonically deformed coals," *Progress in Natural Science*, vol. 19, no. 11, pp. 1455–1466, 2009.

[23] B. Zhang and G. Q. Chen, "Methane emissions by Chinese economy: inventory and embodiment analysis," *Energy Policy*, vol. 38, no. 8, pp. 4304–4316, 2010.

[24] B. Zhang, G. Q. Chen, J. S. Li, and L. Tao, "Methane emissions of energy activities in China 1980–2007," *Renewable and Sustainable Energy Reviews*, vol. 29, pp. 11–21, 2014.

[25] W. Li, P. L. Younger, Y. Cheng et al., "Addressing the $CO_2$ emissions of the world's largest coal producer and consumer: lessons from the Haishiwan coalfield, China," *Energy*, vol. 80, pp. 400–413, 2015.

[26] Y. Liu, F. Wang, H. Tang, and S. Liang, "Well type and pattern optimization method based on fine numerical simulation in coal-bed methane reservoir," *Environmental Earth Sciences*, vol. 73, no. 10, pp. 5877–5890, 2015.

[27] P. Guo, Y. Cheng, K. Jin, and Y. Liu, "The impact of faults on the occurrence of coal bed methane in Renlou coal mine, Huaibei coalfield, China," *Journal of Natural Gas Science and Engineering*, vol. 17, pp. 151–158, 2014.